Fabrication of Nitrogen-Doped Porous Carbon Adsorbents for Highly Efficient Adsorptive Denitrification and Desulfurization

Ding-Ming Xue [a,†], Hai-Dong Zhang [b,†], Jun Zhang [a], Cong-Cong Sun [a], Yu-Chao Wang [c], Xiao-Qin Liu [c,*], Ya-Qi Hou [d,*], Yi-Jun Zhang [e,*]

[a] *Nanjing Institute of Environmental Sciences, Ministry of Ecology and Environment, Nanjing 210042, China*

[b] *Shandong Solid Waste and Hazardous Chemicals Pollution Control Center, Jinan, 250012, China*

[c] *State Key Laboratory of Materials-Oriented Chemical Engineering, College of Chemical Engineering, Nanjing Tech University, Nanjing 211816, China*

[d] *Institute of Flexible Electronics (IFE, Future Technologies), Xiang'an Campus, Xiamen University, Xiamen 361102, China*

[e] *Institut de Science des Matériaux de Mulhouse (IS2M, CNRS-UHA, UMR 7361), F-68057 Mulhouse, France*

[†]Ding-Ming Xue and Hai-Dong Zhang contributed equally to this work.

*Corresponding authors E-mail: liuxq@njtech.edu.cn (X.-Q. Liu); ifeyqhou@xmu.edu.cn (Y.-Q. Hou); yijun.zhang@uha.fr (Y.-J. Zhang).

General characterization

Thermogravimetric analysis (TG) was performed through a synchronous thermal analyzer (NETZSCH STA). The testing conditions involved a high-purity N_2 atmosphere and the temperature was ramped at a rate of 10 ^oC min^{-1} up to 800 ^oC. The Fourier Transform Infrared Spectrometer (FTIR) measurements were performed on an AVATAR-360 infrared spectrometer using the KBr pellet technique and the measurement was conducted over a wavenumber range of 4000 to 650 cm^{-1}. XRD patterns of the materials were gained in the 2ϑ range from 5 ^{o} to 80 ^{o} on a D8 Advance diffractometer with Cu-Kα radiation at 40 kV and 40 mA. Raman Spectra were performed on HR800 UV Raman (France) with an excitation light source wavelength of 514 nm. The FEI Nova SEM 450 cold Field Emission Scanning Electron Microscope (FE-SEM) was used to observe the morphologies of the materials. Transmission Electron Microscope (TEM) and Energy Dispersive X-Ray Mapping (EDX-Mapping) were executed on a FEI TecnaiG2 F20 electron microscope 300 kV. Elemental analysis (EA) of the materials was performed on the Elementar Vario EL instrument (Germany). X-Ray photoelectron spectroscopy (XPS) analysis was performed with an Al Kα at 10 kV and 30 mA. The N_2 adsorption isotherm was measured at 77 K using an BELSORP MAXII instrument. Ahead of analysis, the samples were degassed at 150 ^oC for 4 h under vacuum. The specific surface area was computed at relative pressure ranging from 0.04 to 0.25 through Brunauer-Emmet-Teller (BET) equation. The total volume was calculated from the amount adsorbed at a relative pressure of 0.99. The pore size distribution was evaluated by Non-local Density Functional Theory (NLDFT) model.

Liquid Phase Adsorption Experimental Section

Model Fuel Configuration

The model fuel was used with isooctane as the solvent, and 4A molecular sieves after high-temperature calcination were used for dehydration of isooctane. According to Equation (S1), adsorbates and isooctane were mixed in a certain ratio and ultrasonication was used to obtain homogeneous solution. The initial concentrations of model fuel were 150, 350, 550, 750, 1000, 1250 and 1500 ppmw, respectively. For

competitive adsorption tests, the model fuel mixture consisted of toluene and isooctane in a volume ratio of 15: 85.

$$C = \frac{m(^{M_a}/_{M_m}) \times 10^6}{\rho V + m} \quad \text{(Equation S1)}$$

Where C is the initial concentration of model fuel (ppmw); V is the volume of model fuel (mL); m is the mass of adsorbate (g); ρ is the density of model fuel (g mL^{-1}); M_a is the relative atomic mass of the adsorbate; M_m is the relative molecular mass of the adsorbate.

Liquid Phase Adsorption Analysis

The adsorbate and isooctane were mixed homogenously under dry and room temperature conditions. The static adsorption isotherm was estimated by using the Batch method and tested by external standard method on a gas chromatography (7890A, Agilent) with a CP-Wax 52 CB capillary column ($30\ m \times 0.32\ mm \times 0.5\ \mu m$), injector temperature 280 °C and detector temperature 300 °C.

Regeneration of the adsorbent is an important performance indicator. After each test, the supernatant was poured out and the adsorbent was washed with a mixture of ethanol/water, dried, and then activated again for reuse.

Liquid Phase Adsorption Calculation

The calculation of liquid phase adsorption was calculated by Equation (S2):

$$Q_e = \frac{\rho V(C_0 - C_e)}{1000Mm} \quad \text{(Equation S2)}$$

Where Q_e is the adsorption capacity of adsorbent (mmol g^{-1}); C_0 is the initial concentration of the model fuel (ppmw); C_e is the equilibrium concentration of the model fuel (ppmw); ρ is the density of model fuel (g mL^{-1}); V is the volume of model fuel (mL); m is the mass of adsorbate (g); M is the relative atomic mass of sulfur or nitrogen (g mol^{-1})

The liquid phase adsorption isotherm fitting was performed by Freundlich Equation (S3):

$$Q_{ads} = K_F C_e^{\frac{1}{n}} \quad \text{(Equation S3)}$$

Where Q_{ads} is the adsorption capacity at equilibrium (mmol g^{-1}); C_e is the concentration of model fuel at equilibrium adsorption; K_F is Freundlich constant; n is empirical constant.

The adsorption heat of the adsorbent was calculated by using the Clausius-Clapeyron Equation (S4):

$$\Delta H_{ad} = -RT^2\left(\frac{\partial lnC_e}{\partial T}\right) \quad \text{(Equation S4)}$$

Where ΔH_{ad} is adsorption heat (kJ mol^{-1}); C_e is the concentration of model fuel at equilibrium adsorption; R is ideal gas constant, (8.314 J mol^{-1} K^{-1}); T is the adsorption temperature (K).

Density Functional Theory (DFT) Calculation

The structural optimizations and binding energy calculations were carried out using the CP2K software package (version 2023.1). The initial structures of different NPC-Ts with various adsorbates, including 4,6-DMDBT, thiophene, indole, and quinoline, are illustrated in Fig. S7. Graphene supercell models doped with different forms of N are constructed to represent the surfaces of the respective NPC-Ts. A 20 Å vacuum layer was normally added to the surface to eliminate the artificial interactions between periodic images. The optimized structures of the NPC-Ts-adsorbate complexes are depicted in Fig. 7 (in section 3.4 Adsorption Mechanism).

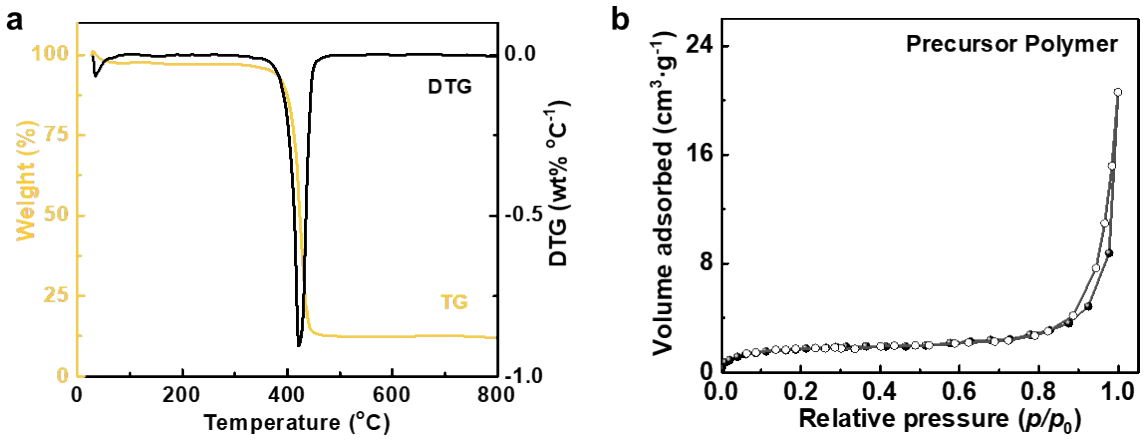

Fig. S1. (a) TG and DTG curves of precursor polymer (under N_2). (b) N_2 adsorption-desorption isotherms of precursor polymer at 77 K.

Table S1. Comparisons of 4,6-DMDBT adsorption capacity on various adsorbents.

Adsorbents	S_{BET} ($m^2\ g^{-1}$)	4,6-DMDBT Capacity ($mmol\ g^{-1}$)	C_0 (ppmw)	Ref.
BN-C-0.5	858	1.1	500	[1]
BCN-Cu-0.06	1367	1.26	500	[2]
MIL-101(Cr)	2322	0.22	550	[3]
Activated Carbon	1843	0.34	343.4	[4]
Cou@M-2-UV	2190	0.53	550	[5]
Modified Silica	480	0.12	2200	[6]
BN-C_3	807	1.15	400	[7]
UMCM-150	3100	1.28	600	[8]
UMCM-152	3480	2.56	600	[9]
NPC-700	2011	2.68	1000	This work
NPC-700	2011	2.04	550	This work

Table S2. Comparisons of indole and quinoline adsorption capacity on various adsorbents

Adsorbents	S_{BET} ($m^2\ g^{-1}$)	Indole Capacity (mmol g^{-1})	Quinoline Capacity (mmol g^{-1})	C_0 (ppmw)	Ref.
Al-NDC@GO-4	348	4.16	2.87	2500	[10]
Ce0.2Y	706	1.51	1.81	1845.1	[11]
ED-MIL-100(Cr)	1395	0.34	0.58	1000	[12]
CuCl/MIL-100(Cr)	1310	1.46	3.54	1000	[13]
UiO-66-NH_3^+	742	1.97	1.69	1000	[14]
(Cr)MIL-101-SO_3Ag	1253	3.05	3.10	1000	[15]
UiO-66-NH-SO_3H	794	1.71	1.16	1000	[16]
Cu_2O/MDC-K	2023	2.74	2.64	1000	[17]
P-MIL-125-NH_2(100)	1413	4.97	4.22	1000	[18]
P-pANI-5	2495	4.70	3.88	1000	[19]
OC-ED-A-M101	1356	6.09	4.55	500	[20]
NPC-700	2011	8.33	3.00	1000	This work

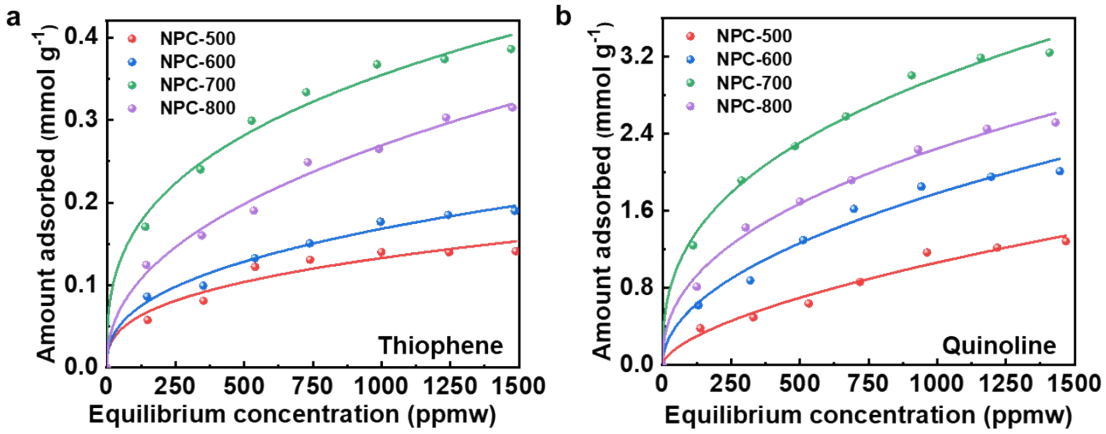

Fig. S2. (a) Thiophene adsorption isotherms and (b) Quinoline adsorption isotherms of NPC-Ts.

Table S3. Comparisons of thiophene adsorption capacity on various adsorbents.

Adsorbents	S_{BET} ($m^2\ g^{-1}$)	Thiophene Capacity (mmol g^{-1})	C_0 (ppmw)	Ref.
BL-ZSM-5	307	0.01	100	[21]
B3	253	0.06	120	[22]
CeAlSBA-15(NH4+)	308	0.10	50	[23]
SBA-15	850	0.15	200	[24]
20Ni-MIL-101	1570	0.30	700	[25]
NaX	717	0.35	250	[26]
Cu(I)Y@P (3.1%)	728	0.53	550	[27]
Ag/TiO_x-Al_2O_3	209	0.61	3500	[28]
HKUST-1/Fe_3O_4	1356	0.62	650	[29]
Cu(I)/SBA-15(40)	754	0.90	1000	[30]
Ag_2O/SiO_2-TiO_2-50	761	0.36	2000	[31]
Cu(I)Y-5.30	488	0.43	1000	[32]
PAN-CNFs-700	170	1.94	800	[33]
NPC-700	2011	0.36	1000	This work

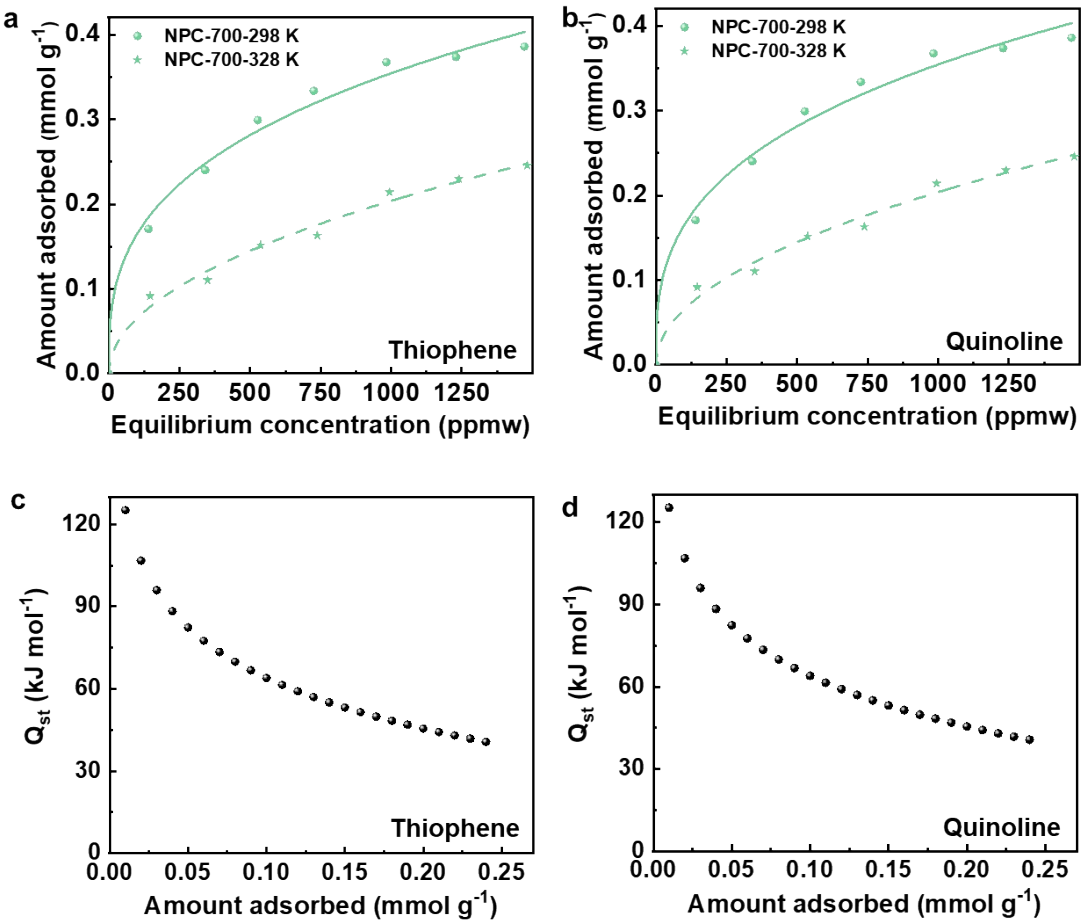

Fig. S3. (a, b) Thiophene and quinoline adsorption isotherms of NPC-700 at 298 K and 328 K. (c, d) Thiophene and quinoline isosteric heat of NPC-700 at different adsorption amount.

Table S4. Fitting parameters of Freundlich model on the NPC-700 at 298 K and 328 K.

Adsorbate	**Thiophene**			**Quinoline**		
***T* (K)**	***k***	***n***	***R²***	***k***	***n***	***R²***
298	0.03557	3.00451	0.99021	0.23422	2.7151	0.99454
328	0.00671	2.02328	0.98781	0.07254	2.1435	0.99406

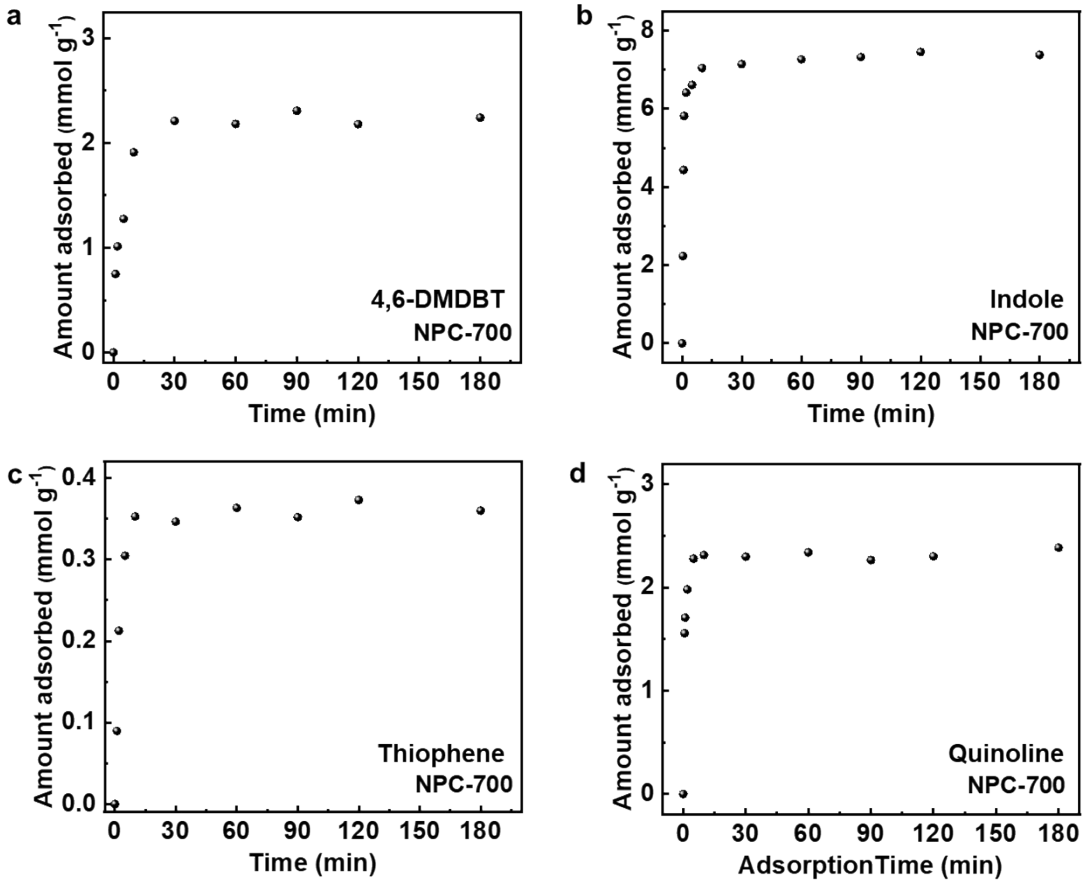

Fig. S4. Effect of the contact time on different adsorption for NPC-700: (a) 4,6-DMDBT, (b) indole, (c) thiophene, and (d) quinoline.

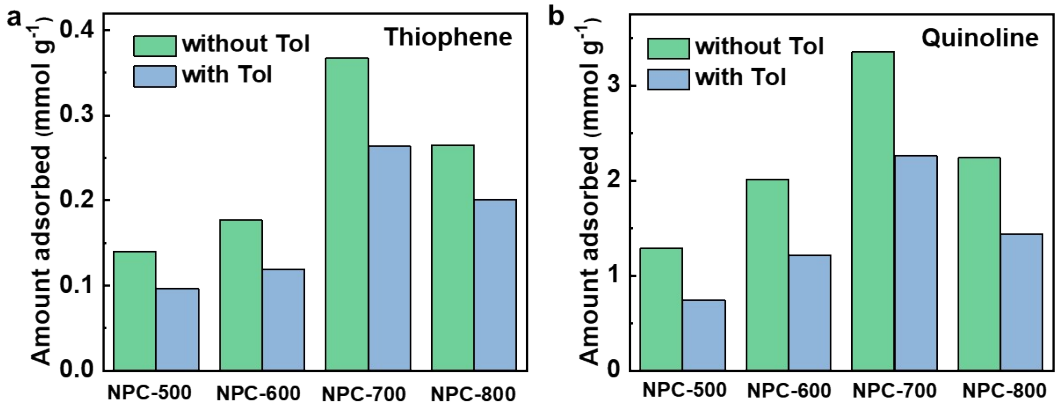

Fig. S5. Completive adsorption on the NPC-Ts for (a) thiophene and (b) quinoline.

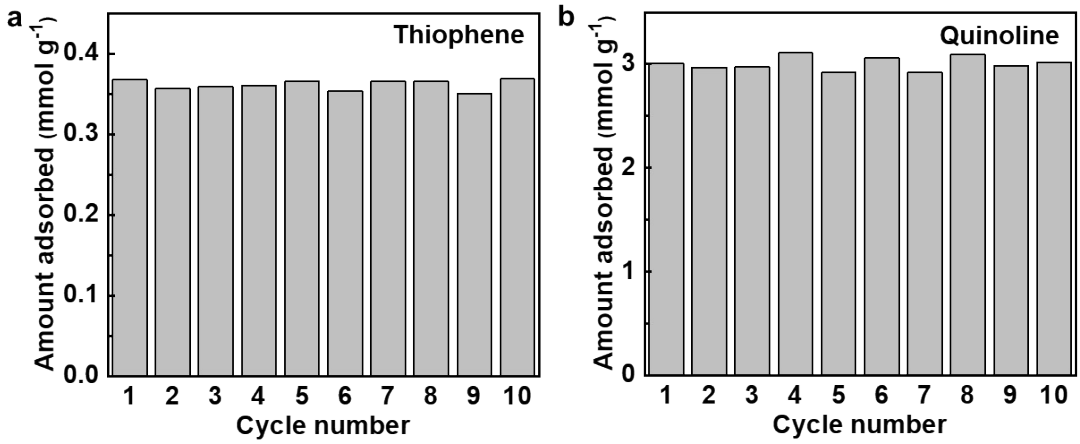

Fig. S6. Reusability of NPC-700 for (a) thiophene and (b) quinoline.

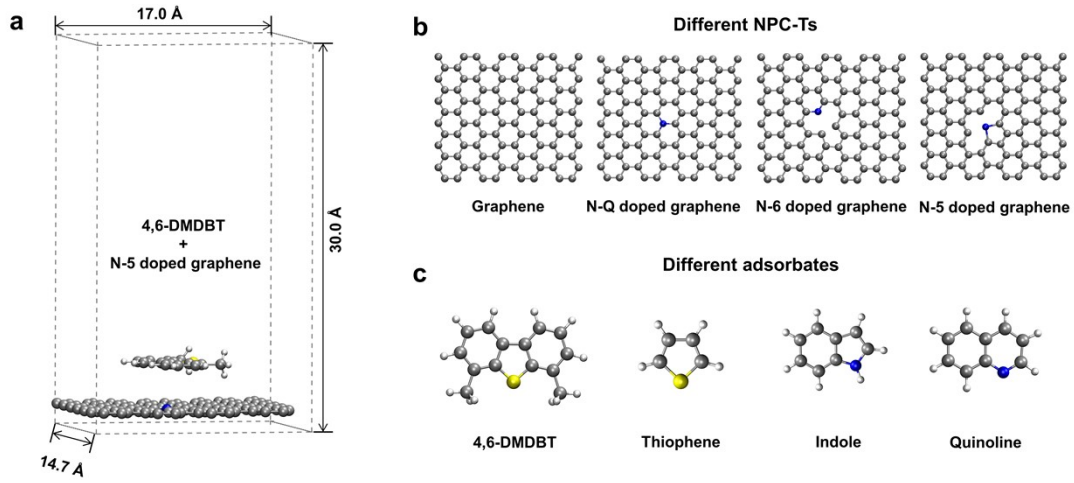

Fig. S7 (a) Initial configurations of NPC-Ts-adsorbate complexes. (b) The configurations of carbon materials. (c) The configurations of different adsorbates.

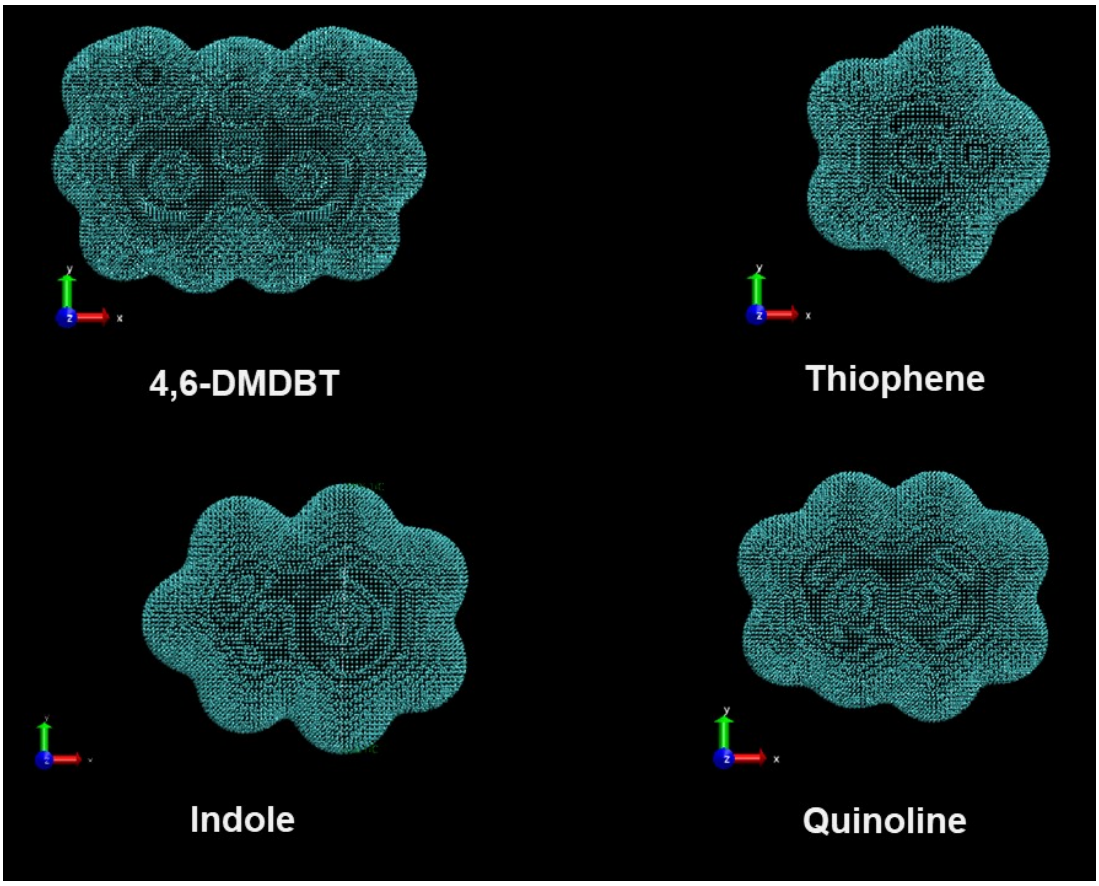

Fig. S8. Theoretical calculation of adsorbate molecular size.

Table S5. Molecular size of different adsorbates

	X (Å)	Y (Å)	Z (Å)
4,6-DMDBT	11.573	8.212	4.325
Thiophene	6.637	6.988	4.151
Indole	9.035	7.505	3.903
Quinoline	9.238	7.45	3.823

References

1. L. Mu, J. Luo, C. Wang, J. Liu, Y. Zou, X. Li, Y. Huang, P. Wu, H. Ji and W. Zhu, BN/ZIF-8 derived carbon hybrid materials for adsorptive desulfurization: Insights into adsorptive property and reaction kinetics, *Fuel*, 2021, **288**, 119685-119692.
2. Y. Zhang, H. Ran, X. Liu, X. Zhang, J. Yin, J. Zhang, J. He, H. Li and H. Li, Cu-doped BCN nanofibers for highly selective adsorption desulfurization through S-Cu coordination and π-π interaction, *Sep. Purif. Technol.*, 2023, **318**, 123963-123973.
3. Y.-X. Li, W.-J. Jiang, P. Tan, X.-Q. Liu, D.-Y. Zhang and L.-B. Sun, What matters to the adsorptive desulfurization performance of metal-organic frameworks?, *J. Phys. Chem. C*, 2015, **119**, 21969-21977.
4. J. H. Kim, X. Ma, A. Zhou and C. Song, Ultra-deep desulfurization and denitrogenation of diesel fuel by selective adsorption over three different adsorbents: A study on adsorptive selectivity and mechanism, *Catalysis Today*, 2006, **111**, 74-83.
5. J. Zhu, S. C. Qi, X. Q. Liu and L. B. Sun, Coumarin-functionalized metal-organic frameworks: adsorbents with photo-responsive active sites for adsorptive desulfurization, *Chem. Commun.*, 2023, **59**, 8700-8703.
6. X. Wei, S. M. Husson, M. Mello and D. Chinn, Removal of branched dibenzothiophenes from hydrocarbon mixtures via charge transfer complexes with a tapa-functionalized adsorbent, *Ind. Eng. Chem. Res.*, 2008, **47**, 4448-4454.
7. J. Xiong, L. Yang, Y. Chao, J. Pang, P. Wu, M. Zhang, W. Zhu and H. Li, A large number of low coordinated atoms in boron nitride for outstanding adsorptive desulfurization performance, *Green Chem.*, 2016, **18**, 3040-3047.
8. C. K. A, W.-F. A. G, M. A. J and L. Phase, Liquid phase adsorption by microporous coordination polymers: removal of organosulfur compounds, *J. Am. Chem. Soc.*, 2008, **130**, 6938-6939.
9. J. K. Schnobrich, O. Lebel, K. A. Cychosz, A. Dailly, A. G. Wong-Foy and A. J. Matzger, Linker-directed vertex desymmetrization for the production of coordination polymers with high porosity, *J. Am. Chem. Soc.*, 2010, **132**, 13941-13948.
10. X. Hu, Z. Zuhra, S. Ali, Y. Zhou, L. Zhang, X. Duan and Z. Zhao, Adsorptive denitrogenation of model oil by MOF(Al)@GO composites: remarkable adsorption capacity and high selectivity, *New J. Chem.*, 2023, **47**, 3306-3311.
11. J. Zhang, L. Huang, X. Lin, Y. Wang, Y. Yu and T. Qi, Effective Adsorptive Denitrogenation from Model Fuels over CeY Zeolite, *Ind. Eng. Chem, Res.*, 2022, **61**, 14586-14597.
12. I. Ahmed, Z. Hasan, N. A. Khan and S. H. Jhung, Adsorptive denitrogenation of model fuels with porous metal-organic frameworks (MOFs): Effect of acidity and basicity of MOFs, *Appl. Catal. B-Environ.*, 2013, **129**, 123-129.
13. I. Ahmed and S. H. Jhung, Adsorptive denitrogenation of model fuel with CuCl-loaded metal-organic frameworks (MOFs), *Chem. Eng. J.*, 2014, **251**, 35-42.
14. M. Sarker, H. J. An and S. H. Jhung, Adsorptive removal of indole and quinoline from model fuel over various UiO-66s: quantitative contributions of H-bonding and acid-base interactions to adsorption, *J. Phys. Chem. C*, 2018, **122**, 4532-4539.
15. H. She, X. Ma and G. Chang, Highly efficient and selective removal of N-heterocyclic aromatic contaminants from liquid fuels in a Ag(I) functionalized metal-organic

framework: Contribution of multiple interaction sites, *J. Colloid Interface Sci.*, 2018, **518**, 149-155.

16. I. Ahmed, N. A. Khan and S. H. Jhung, Adsorptive denitrogenation of model fuel by functionalized UiO-66 with acidic and basic moieties, *Chem. Eng. J.*, 2017, **321**, 40-47.

17. N. A. Khan, S. Shin and S. Hwa Jhung, Cu2O-incorporated MAF-6-derived highly porous carbons for the adsorptive denitrogenation of liquid fuel, *Chem. Eng. J.*, 2020, **381**, 122675-122681.

18. I. Ahmed, N. A. Khan, J. W. Yoon, J. S. Chang and S. H. Jhung, Protonated MIL-125-NH_2: remarkable adsorbent for the removal of quinoline and indole from liquid fuel, *ACS Appl. Mater. Interfaces*, 2017, **9**, 20938-20946.

19. N. A. Khan, D. K. Yoo and S. H. Jhung, Polyaniline-encapsulated metal-organic framework MIL-101: adsorbent with record-high adsorption capacity for the removal of both basic quinoline and neutral indole from liquid fuel, *ACS Appl. Mater. Interfaces*, 2018, **10**, 35639-35646.

20. M. M. H. Mondol, B. N. Bhadra, J. M. Park and S. H. Jhung, A remarkable adsorbent for removal of nitrogenous compounds from fuel: A metal-organic framework functionalized both on metal and ligand, *Chem. Eng. J.*, 2021, **404**, 126491.

21. Y. Xiao, Q. Xue, K. Zhu and G. He, Enhanced performance of adsorptive removal of thiophene from model fuel over micro-mesoporous binderless ZSM-5 prepared by in situ crystallization, *Energy Fuels*, 2020, **34**, 5623-5633.

22. S. Uzunova, L. Minchev, I. Uzunov and V. Toteva, Efficient adsorption of thiophene from model fuel by pyrolysed rice husks: factors of influence, *Chemistry and Ecology*, 2016, **32**, 976-987.

23. Y. Zu, L. Guan, Z. Guo, C. Huang, D. He and Y. Mei, Deep removal of thiophene and benzothiophene in low-sulfur fuels over the efficient CeAlSBA-15 adsorbent synthesized by sequential alumination and cerium incorporation, *Chem. Eng. J.*, 2021, **416**, 127984.

24. Y. Yang, G. Lv, J. Li, W. Guo and Y. Zhang, Synthesis of ceria nanorods as adsorbent for the adsorption desulfurization of gasoline fuel, *J. Alloys Compd.*, 2018, **747**, 189-196.

25. S. Aslam, F. Subhan, Z. Yan, U. J. Etim and J. Zeng, Dispersion of nickel nanoparticles in the cages of metal-organic framework: An efficient sorbent for adsorptive removal of thiophene, *Chem. Eng. J.*, 2017, **315**, 469-480.

26. Y. Xu, Z. Zhong, S. Lu and Y. Zeng, Monte Carlo Simulations of Adsorption of Thiophene/Benzene in NaX and NaY Zeolites from Model Fuel, *Ind. Eng. Chem, Res.*, 2020, **59**, 15742-15751.

27. Y. X. Li, J. X. Shen, S. S. Peng, J. K. Zhang, J. Wu, X. Q. Liu and L. B. Sun, Enhancing oxidation resistance of Cu(I) by tailoring microenvironment in zeolites for efficient adsorptive desulfurization, *Nat. Commun.*, 2020, **11**, 3206-3214.

28. A. H. M. S. Hussain, H. Yang and B. J. Tatarchuk, Investigation of organosulfur adsorption pathways from liquid fuels onto Ag/TiOx-Al_2O_3 adsorbents at ambient conditions, *Energy Fuels*, 2013, **27**, 4353-4362.

29. P. Tan, X. Y. Xie, X. Q. Liu, T. Pan, C. Gu, P. F. Chen, J. Y. Zhou, Y. c. Pan and L. B. Sun, Fabrication of magnetically responsive HKUST-1/Fe_3O_4 composites by dry gel

conversion for deep desulfurization and denitrogenation, *J. Hazard. Mater.*, 2017, **321**, 344-352.

30. L. Kong, T. Zhang, R. Yao, Y. Zeng, L. Zhang and P. Jian, Adsorptive desulfurization of fuels with Cu(I)/SBA-15 via low-temperature reduction, *Micropor. Mesopor. Mat.*, 2017, **251**, 69-76.

31. L. Yin, B. Zhang, J. Zhou, J. Xu, W. Gong, J. Gao, W. Ning, Z. Zhang and W. H. Yu, High Adsorption Performance of Bimetal Ag,Ti-Doped SiO2 Aerogel Composites for the Removal of Thiophenic Compounds from Model Fuels, *J. Chem. Eng. Data*, 2020, **65**, 4924-4934.

32. W. Cui, J. Wang, Y. Xu, Z. Cao and Y. Zeng, Stability improvement of FAU zeolites ion-exchanged with copper-ammonia solution for the removal of thiophene and benzothiophene from model fuel, *J. Chem. Eng. Data*, 2019, **64**, 5439-5447.

33. X. L. Sun, Z. Liu and Z. L. Cheng, Design and fabrication of in-situ N-doped paper-like carbon nanofiber film for thiophene removal from a liquid model fuel, *Journal of Hazardous Materials*, 2020, **389**, 121879-121888.